Effect of carbon content on structural, mechanical and tribological properties of Cr-V-C-N coatings

Linda Aissani [a,b], Akram Alhussein [c,*], Ahlam Belgroune [b,c], Corinne Nouveau [d], Elia Zgheib [c], Regis Barille [e], Alex Montagne [f]

[a] Matersciences Department, Abbes Laghrour-Khenchela University P.O1252, 40004, Algeria
[b] Laboratory of Active Components and Materials, Larbi Ben M'Hidi University, Oum El Bouaghi 04000, Algeria
[c] LASMIS, Université de Technologie de Troyes, Pôle Technologique Sud Champagne, 26 Rue Lavoisier, 52800 Nogent, France
[d] Arts et Metiers Institute of Technology, LABOMAP, HESAM Université, F-71250 Cluny, France
[e] Moltech Anjou, Université Angers/CNRS UMR 62002, Bd Lavoisier, 49045 Angers cedex, France
[f] Arts et Metiers Institute of Technology, MSMP, HESAM Université, F-59000 Lille, France

Keywords:
Cr–V–C–N coating
Steel
Magnetron sputtering
Wear resistance
Nanoindentation
Microstructure analysis
Surface topography

A B S T R A C T

Cr-V-C-N thin films were deposited on XC100 steel and Si(100) wafers by a radio frequency magnetron sputtering technique using chromium and vanadium targets in an $Ar/N_2/CH_4$ mixture atmosphere. The microstructure, mechanical and tribological properties of coatings were investigated as a function of carbon content.

It has been found that the quaternary Cr-V-C-N coatings containing a low percentage of carbon ($\leq$ 12.4 at.%) exhibited a mixture of chromium and vanadium nitrides nano-sized crystallite phases. The coatings containing a high carbon content (> 25 at.%) were consisted of nitride and carbide phases, where the large carbon atoms inserted through CrN and VN.

Mechanical properties of the Cr-V-C-N coatings were influenced by the carbon addition. The maximum hardness value of 28.3 GPa was obtained for the coating containing 28 at.% of carbon which is related to the adhesion strength enhanced by the formation of carbide and nitride mixture. Addition of carbon into the Cr-V-N coating led to significantly decrease its friction coefficient from 0.63 to 0.47. The formation of carbides through the dispersion of carbon in the grains effectively improved the density of the Cr-V-C-N coatings so that the coating deposited under a high CH_4 flow rate exhibited a better wear resistance than the other Cr-V-N and Cr-V-C coatings.

1. Introduction

Chromium-based hard coatings have attracted a lot of attentions comparing to the other transition metal nitride coatings, due to their excellent properties such as high hardness, high melting point and good resistance to wear and corrosion [1–4]. Cr-N is one of these coatings deposited using magnetron sputtering technique [2,3]. This technique offers good adhesion of coating to the steel substrates at relatively low deposition temperature. However, the Cr-N coating could not satisfy the work requirements under extreme conditions because its high friction coefficient (0.53) and low wear resistance [5]. Furthermore, the enhancement of Cr-N hardness is crucial to improve its tribological behavior. Thus, the reduction of Cr-N friction coefficient is the main issue in order to develop its resistance in the industrial environment.

The incorporation of some elements like carbon during the deposition of transition metal nitride coatings is possible to obtain ternary or quaternary coatings with considerable changes in the structural and chemical characteristics: crystalline structure, chemical bonding, grain size and shape. The carbon with sp, sp^2 and sp^3 binding characteristics leads to enhance the physical and mechanical properties of Cr-C-N coatings. Previous studies have confirmed a great interest in this alloy [5,6].

Carbon as a self-lubricated solid material with a low friction coefficient has also been used in industry. The incorporation of carbon through the Cr-N coatings may reduce their friction coefficient [5–7]. The Cr–C–N coatings have been especially investigated for various tools. The enhancement of mechanical and wear properties of Cr-C-N coatings, as compared to binary Cr-N, were attributed to the solid solution

* Corresponding author.
E-mail address: akram.alhussein@utt.fr (A. Alhussein).

https://doi.org/10.1016/j.tsf.2021.138782

hardening made by carbon atoms [5–7]. E. Contreras et al. [8] have reported an important reduction in the friction coefficient of CrN from 0.6 to 0.25 by controlling the carbon content in the coating. This coating was deposited by magnetron sputtering and its tribological behavior was studied against Si_3N_4 balls in dry conditions. The improved tribological behavior can be attributed to the high carbon content in the coating (89.2 at. % of C) and to increase the grain boundaries, which leads to the formation of amorphous carbon. Nevertheless, the increase of coating hardness results in the enhancement of wear resistance [9]. During the dry ball-on-disk tests, the Cr-C-N coatings constantly exhibit a lower friction coefficient than the CrN coatings [5,10]. However, under some extreme conditions like high temperature with conventional lubricant, these coatings become soft and fail because of their severe wear [10].

It is known that the hardness is one of the most important mechanical properties influencing the wear resistance of materials. For tribological applications, it is important to decrease the friction coefficient and maintain high strength and hardness of a coating. For this reason, many studies have been carried out in order to enhance the performance of carbonitride coatings by incorporating a third element such as Al, Si, Cr, V, or Ti. It is well understood that the good performance is strongly related to not only the elemental composition but also the formation of unique microstructure (nanocomposite or solid-solution) [5,10].

Among these elements, particular attention has been given to the nitride coatings containing vanadium, which showed a high hardness and good wear, oxidation and corrosion resistance [11–14]. S. He et al. [14] have found that the mechanical and tribological properties of Ti–W–V-N coatings had a great improvement compared to the ternary Ti–W-N coating in the temperature range 300–700 °C by the formation of the substitutional solid solution of fcc-(Ti, W, V)N.

H. Ju et al. [11] have studied the influence of vanadium content on the Nb–V–Si–N coatings and found that the good tribological properties were obtained with the formation of lubricant Nb_2O_5 and V_2O_5 oxides at the surface (at 200 °C). F. Fernandes et al. [12] have found that the addition of V into Ti-Si-N coatings led to enhance their mechanical properties and resistance to wear and oxidation. This combination of properties has been achieved by the formation of an external V_2O_5 oxide, thin top layer, during corrosion or oxidation. In addition to the formation of these vanadium oxides, some authors relate the good wear-corrosion resistance of the coatings to the dense structure, which prevents oxygen diffusion along the grain boundaries [11–14].

Cr-N coatings with carbon and vanadium atoms embedded in a nanocrystalline Cr-V-N and Cr-C-N matrix. The structure of these coatings provides an extremely high hardness to these ternary systems and can prevent dislocation movements and micro-cracking, thereby improving their mechanical and tribological properties [15,16].

Several recent investigations have shown that the addition of carbon in the presence of vanadium reduces the grain size, which leads to enhance the hardness and strength of material as described by Hall–Petch relationship [5]. W.Y. Ho et al. [17] have reported that addition of carbon into Ti-V-C-N coating led to achieve high hardness, and best wear resistance and thermal stability. Furthermore, recent work performed by L.R. Constantin et al. [18] presented a correlation between the structures, tribological properties and corrosion of Zr–Cr–Si–C–N coatings. They showed that the improvement of microstructure by the formation of carbides, as well as friction, wear and anti-corrosive performance of Zr-C-N and Zr–Cr–Si–C–N coatings was achieved by the presence of C–Metal, N–Metal, C-C and N–C chemical bonds.

In the literature, we can find few researches focused on studying the chromium-based carbonitride quaternary system. Heo et al. [16] investigated Cr-V-N and Cr-V-C-N coatings deposited on steel substrates. They studied the influence of carbon content on structure, mechanical properties and wear resistance of sputtered V-C-N coatings. They found that the Cr–V–C–N coating, containing 10.4 at. % of V, showed a fine composite microstructure consisting of nanosized crystallites of (Cr, V), (C, N) and amorphous V-C-N phases and presented a higher hardness of 34 GPa than that of a Cr(C, N) coating (27 GPa). Moreover, the friction coefficient of the Cr–V–C–N coating was lower ($\mu = 0.27$) than this of Cr-C-N coating ($\mu = 0.38$), which is largely dependent on the vanadium content and tribo-chemical reaction during the wear process. However, the corrosion resistance of Cr-V-C-N coatings has not yet been thoroughly studied, due to the synergy problems highly observed in steel devices [16].

In this paper, we present the combination effect of nitrogen and carbon on the structure and properties of the quaternary Cr-V-C-N coatings deposited by a radio frequency magnetron sputtering technique. In addition, we present the correlation between the structure, the hardness and the tribological performance. The results will be compared with those reported in the literature. The results of this work will support further research for the enhancement of mechanical properties and wear resistance of coatings used in an industrial environment.

2. Experimental details

2.1. Deposition procedure

A series of Cr-V-C-N coatings with different C contents was deposited using a radio frequency reactive magnetron sputtering machine (NORDIKO type 3500, 13.56 MHz, 1.25 kW). High purity Cr (99.99%) and V (99.99%) circular targets of 10.6 cm diameter were used. The substrates-targets distance was fixed at 80 mm and with an angle of +45° (Cr) and -45° (V) from the normal to obtain coatings with uniform thickness and a good deposition rate. Coatings were deposited on Si (100) wafers (10 × 10 × 0.38 mm) and XC100 steel (Ø 12 × 3 mm) substrates. The coated Si wafers were used to measure the coating chemical composition, thickness and surface roughness and the coated steel substrates were used to evaluate the mechanical properties and tribological performance. The steel samples were polished using grit SiC emery papers with a grit size of 300, 600, 1000 and 1200, and subsequently polished to a mirror finish with a 0.5 μm alumina solution to obtain a low surface roughness. Thereafter, the substrates were cleaned in an ultrasonic bath of acetone and ethanol solutions for 10 min. Prior to the deposition procedure, the chamber was evacuated down to a low pressure of 2×10^{-5}Pa. The substrates and targets were etched by Ar ions for 10 min and surface oxide layers and impurities were removed. The cleaning step was performed with the following conditions: 80 sccm argon flow rate, 0.4 Pa working pressure, −700 V bias voltage and 250 W power (-500 V) applied to chrome and vanadium targets.

All Cr-V-C-N coatings were deposited at 150 °C for 2 h, 0.4 Pa working pressure and the powers (voltages) applied to Cr and V targets were fixed at 650 W (-900 V) and 550 W (-900 V), respectively. The deposition of Cr-V-C and Cr-V-N coatings was carried out in a mixture atmosphere of two gases, respectively (10 sccm CH_4 + 90 sccm Ar) and (20 sccm N_2 + 80 sccm Ar), as shown in Table 1. Cr-V-C-N thin films deposition was performed in Ar/N2/CH4 discharge while varying N_2 and CH_4 flow rate in the 15–8 sccm range and 5–12 sccm range, respectively. The total volume of gases flow, injected in the deposition chamber, was kept constant at 100 sccm.

2.2. Coatings characterization

The elemental chemical composition of coatings was measured using an Energy Dispersive Spectroscopy (EDX, Oxford INCA x-act, 15 kV) and X-ray photoelectron spectroscopy (XPS, Riber SIA 100). The coating elemental quantification was obtained by the peak-height ratio relative to a standard using Proza (Phi-Rho-Z) algorithm in EDX technique. The EDX detector has a NORVAR window type of 30 mm^2 active area. In our work, the chemical composition values present the average of three areas (1 mm^2) analyzed for each sample. The XPS operation conditions were 300 W, 20 mA, and 4×10^{-5}Pa at room temperature. The surface contaminants on the coatings were removed by Ar^+ ions bombardment at 5 KeV as a primary energy for 3 min. The XPS measurements were

Table 1
Chemical composition and characteristics of Cr-V-C-N coatings deposited under different (N_2 and CH_4) flow rates. Chemical composition was obtained by EDX, average film thickness and surface roughness were measured with an optical profilometer and an AFM, and crystallite size was calculated from XRD patterns.

Coatings	N_2%	CH_4%	Elemental composition (at.%) Er (N, C, O) ≈ 5 % Er (Cr, V) ≈ 3 %	C/N					(C+N)/ (Cr+V)	Film thickness (nm) (≈ ±20 nm)	Average roughness (nm) (≈ ± 1 nm)	Crystallite Size (nm) (≈ ± 3 %)
			Cr	V	N	C	O					
$Cr_{0.26}V_{0.24}N_{0.44}$	20	-	26.4	24.0	44.4	-	5.2	-	0.88 ±0.07	1620	21.3	193
$Cr_{0.24}V_{0.21}C_{0.12}N_{0.36}$	15	5	24.1	21.5	36.0	12.4	6.0	0.34 ±0.03	1.06 ± 0.08	1340	18.0	142
$Cr_{0.23}V_{0.20}C_{0.24}N_{0.27}$	12	8	23.5	20.4	27.2	24.0	4.9	0.88 ±0.07	1.17 ± 0.09	1310	15.1	82
$Cr_{0.22}V_{0.21}C_{0.28}N_{0.24}$	10	10	22.4	21.2	24.0	28.0	4.4	1.16 ±0.09	1.19 ± 0.09	1260	10.5	43
$Cr_{0.21}V_{0.20}C_{0.32}N_{0.22}$	8	12	21.4	20.2	22.0	32.0	4.4	1.45 ±0.11	1.27 ± 0.10	1230	11.1	46
$Cr_{0.33}V_{0.26}C_{0.34}$	-	10	32.8	26.0	-	34.0	7.2	-	0.58 ± 0.05	1700	42.0	245

performed with Al-Kα irradiation at 1486.6 eV energy.

The crystallographic structures of coatings were analyzed by X-Ray Diffraction (XRD) using a Siemens D500 diffractometer with Co cathode ($Co_{K\alpha}$ radiation $\lambda = 1.78$ Å, 45 kV, 40 mA). A θ–2θ scan was carried out for 2θ diffraction angles ranging from 20° to 80° with a scan step of 0.02° recorded during 2s.

For a dense structure, we can calculate the average particle size by using the corrected physical broadening with the help of Scherrer equation [19]. In our study, the Scherrer equation was used as an approximation to calculate the average crystallite size. The crystallite size was calculated considering the (111) CrN and (200) Cr_7C_3 planes (Eq. 1):

$$D = \frac{0.9\lambda}{\beta\cos\theta} \quad (1)$$

Where 0.9 is a dimensionless shape factor, λ the X-ray wavelength ($\lambda_{Cu} = 0.154$ nm), β (in rad) the line broadening at half the maximum intensity (full width half maximum) and θ the Bragg's angle of (111) CrN and (200) Cr_7C_3 planes.

Raman spectroscopy measurements were carried out using a co-focal (Bruker Senterra) Raman spectrometer, with an excitation laser radiation at 600 nm (applied power was 17 mW). This identification was supported by a reference Raman spectrum of phases expected in Cr-V-C-N coatings.

The cross section images of the coatings were obtained by a scanning electron microscope (SEM, JEOL JSM-5900LV; 10 kV). The coating thickness was determined using an optical profilometer (VEECO, Wyko-NT 1100). The surface roughness of the coatings was measured using an Atomic Force Microscope (AFM 100, APE research) in contact mode with a silicon nitride pyramidal tip of 50 nm radius and applying a 2N normal load.

The residual stresses generated in coatings during the deposition process were calculated with the Stoney's formula [20].

The mechanical properties of the coatings, hardness and Young's modulus, were measured using a Nano Indenter XP (MTS-XP) system in continuous stiffness measurement (CSM). The tests were performed using a diamond Berkovich indenter tip calibrated in fused silica and applying a maximum load of 700 mN. The maximum penetration depth was limited to less than 10% of the coating thickness in order to avoid the effect of the substrate stiffness [13]. The coating hardness (*H*) and Young's modulus (*E*) were calculated following Oliver-Pharr model [5]. For each coating, 5 indents were performed and the average values of E and H were calculated. Indentation curves were described by means of the general methodology for the coatings with about 2 μm thickness [5].

The tribological behavior of the coatings was assessed by sliding wear tests using a tribometer (TRIBO tester) in a ball-on-disc configuration. Tests were carried out using 6 mm 100Cr6 steel balls, with applying a 2 N normal load, a 200 m sliding distance and a 5 cm s^{-1} constant speed. Tests were performed at ambient temperature without any lubricants and with controlling humidity at 23%. The wear rate (K) was calculated by the following equation:

$$K = V/F{\cdot}d \quad (2)$$

Where V is the worn volume, *F* is the normal load and d is the total sliding distance.

The worn track depth and wear rate were determined with an optical profilometer (VEECO, Wyko-NT 1100). The chemical compositions of worn wear tracks were analysed using an SEM-EDX.

3. Results and discussions

3.1. Chemical analysis

Table 1 shows the elemental composition of the coatings obtained by EDX technique. The Cr-V-C-N coatings, with a total carbon content ranging from 12.4 to 34 at.%, were deposited at different (N_2, CH_4) flow rates (Table 1). We can see that injection of CH_4 inside the deposition chamber and increasing its flow rate led to a gradual decrease of chromium from 26.4 to 21.4 at. %, nitrogen from 44.4 to 22 at. % and vanadium from 24 to 20.2 at. %. It has been shown that the elaborated coatings contained a low amount of oxygen in the 4.4–7.2 at.% range, which is due to the residual oxygen in the deposition chamber and the affinity of metallic elements with oxygen [5,21]. The analytical error of the light elements (O and N) was approximately 5 at.% and that of metallic ones (Cr and V) was about 3 at.%. From Table 1, we can see that increasing of C/N and (C+N)/ (Cr+V) ratios led to obtain coatings enriched in carbon. This is due to the relative reduction of nitrogen and increasing of CH_4 flow rate during the deposition procedure carried out at a fixed total working pressure.

Fig. 1 represents the elemental concentration depth profiles of Cr-V-C-N coatings obtained by XPS technique. We can notice that the amount of all elements remained constant from the coating surface toward the substrate. In the interface zone (coating-substrate), chromium, vanadium, carbon and nitrogen contents decreased while the Si content increased. The highest carbon content was 34 at.% for the Cr-V-C film deposited under 10 sccm of CH_4 (Table 1). The XPS profiles confirm the apparent decrease of coating thickness with increasing the CH_4 flow rate, as revealed by SEM observation (Section 3.2). Therefore, the chemical quantification via quantitative elemental concentration depth profiles is in agreement with the EDX analysis (Table 1). There was no significative difference between the elemental composition values measured by both techniques.

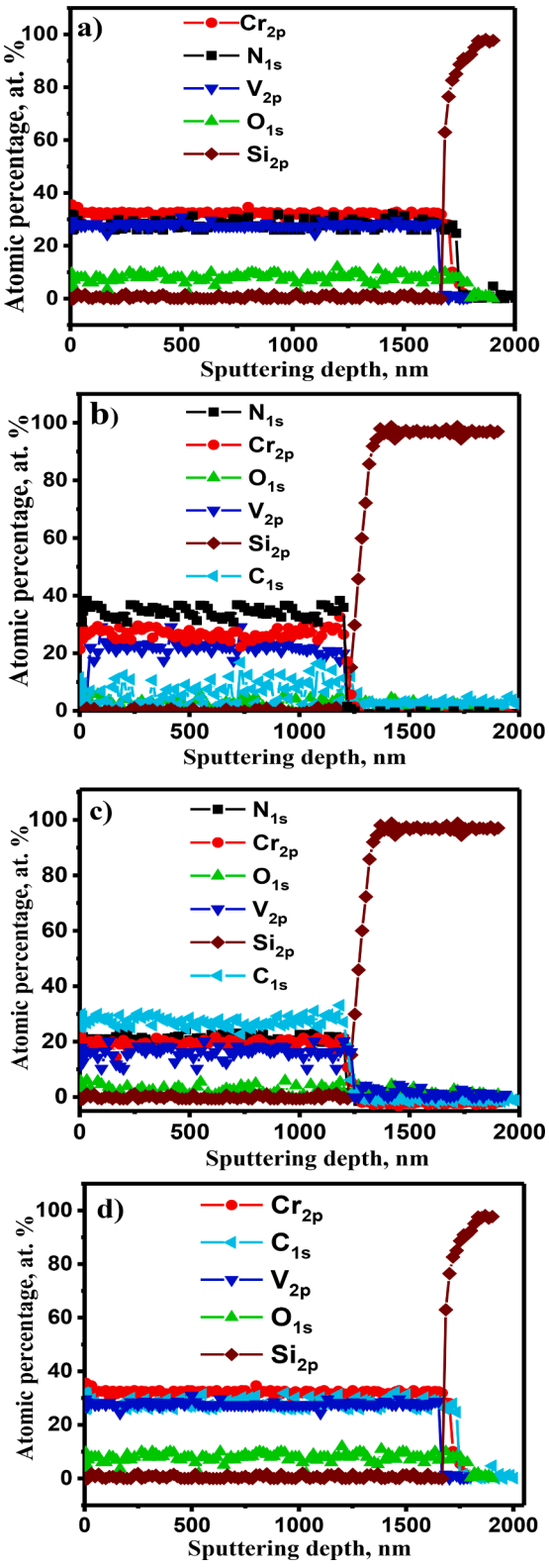

Fig. 1. Quantitative elemental concentration depth profiles of C-V-C-N coatings deposited at: a) (20% N_2, 0% CH_4), b) (15% N_2, 5% CH_4), c) (8% N_2, 12% CH_4), and d) (0 % N_2, 10% CH_4) flow rates.

3.2. *Microstructure analysis*

The analysis of phases in the Cr-V-C-N coatings was performed by means of X-ray diffraction measurements (Fig. 2). The XRD results showed that the coating phases depend on the N_2 and CH_4 flow rates. The JCPDS cards used in this study presenting the different phases formed in the coatings are: 11-0065 (FCC-CrN), 35-0803 (H-Cr_2N), 43-1040 (O-CrO_2), 073-0528 (FCC-VN), 35-0803 (H-V_2N), 19-0334 (O-Cr_2VC_2), 65-1347 (O-Cr_7C_3) and 71-1271 (O-V_2C). As shown from the XRD diffractograms, the Cr-V-N and Cr-V-C-N (deposited under 15 sccm of N_2 and 5 sccm of CH_4) coatings contained a mixture of cubic (CrN, VN) and hexagonal (Cr_2N, V_2N) phases. The phases of these coatings were in agreement with those reported in previous studies [15,21].

Deposition of coatings under high CH_4 flow rate boosted the formation of Cr_7C_3 phase in coatings. The XRD patterns of the Cr-V-C-N coatings, deposited under a gas mixture with at least 8 % of CH_4, present diffraction peaks at 46.09, 51.03, 57.51 and 69.59° corresponding to (200), (123), (220) and (008) planes of orthotropic Cr_7C_3 phase, respectively.

In addition, the XRD patterns of coatings deposited with higher CH_4 flow rate show that the peak corresponding to the (111) VN became broader and the others corresponding to (111) CrN and (200) Cr_7C_3 phases became more intense. We can also notice the presence of other minor phases: (111) Cr_2N, (203) and (202) Cr_7C_3, (121), (123) and (040) V_2C, (400) and (002) Cr_2VC_2. This suggests that the excess C atoms react with the other elemental atoms to form carbide phases. The formed phases were mainly the dominant O-Cr_7C_3 phase as well as the O-V_2C, O-Cr_2VC_2 and O-CrO_2 shown clearly by the XRD patterns of coatings deposited under a flow rate of $CH_4 \geq 8\%$. This is due to the activation energy required to from the (Cr-C) in the chromium carbide coating (178 kJ/mol), which is lower than the energy necessary to form the (V-C) in the vanadium carbide coating (199 kJ/mol) [22].

From Fig. 2, we can see that the XRD patterns of Cr-V-C-N coatings deposited at different N_2 and CH_4 flow rates reveal different intensifications and a slight shift of the FCC-CrN (111) and H-Cr_2N(111) diffraction peak positions to higher angles. The growth of Cr-V-C-N coatings changed from the pronounced (111) CrN to the (200) Cr_7C_3 with increasing the C content (Fig. 2). A similar change in coating growth with increasing C content was also reported in our previous study for the Cr-C-N coatings [5]. With increasing the carbon content in film, we note the disappearance of (111) CrN and the appearance of (200) Cr_7C_3. In fact, the surface energy as well as the strain energy minimization would always favor the carbide stability for a high carbon-containing Cr-V-C-N coating. Since the atomic radii of C and N are much closed, so the carbon atoms easily can replace the nitrogen ones in the CrN lattice. This causes the shift of diffraction peaks to higher angles and the reduction of the lattice parameter of CrN ($a_0 = 4.02$ Å) as compared to the CrN (bulk) powder phase (0.414 nm) reported in the literature, suggesting a reduction of defect-induced lattice strains [21]. However, the lattice parameter was determined for the Cr_7C_3 phase in the (200) direction ($a = 4.58$ Å), which is in good agreement with the result reported by B. Kaplan et al. [23] for the Cr_7C_3 phase prepared by powder metallurgical method ($a = 4.533$ Å). Moreover, it has been reported in our previous work [5] that residual stress has a certain effect on the shift of diffraction peaks: the compressive residual stress in the coatings decreases the lattice spacing and leads to the shift of diffraction peaks to higher angles. This result is also consistent with the XRD patterns of Cr-C-N coatings. Hence, the diffraction peaks still shifted to higher angles may be related to the overlap of (111) (CrN, VN) and (111) (Cr_2N, V_2N) since these diffraction peaks are very close to each other, however the effect of compressive residual stress on the shift of diffraction peaks becomes insignificant.

The Raman spectra of the Cr-V-C-N coatings, deposited under different N_2 and CH_4 flow rates, are presented in Fig. 3. For the coatings deposited under (20 % N_2+ 0 % CH_4) and (15 % N_2 + 5 % CH_4) flow rates, we can identify strong and sharp bands centered at 531 cm^{-1} with other minor peaks at 351, 432, 527, 553 and 613 cm^{-1} associated with CrN and VN phases [3, 20]. The CrN band located at 535 cm^{-1} was sharper and more intense indicating larger grain size for these coatings. However, a notable decrease in their intensity can be observed, which is

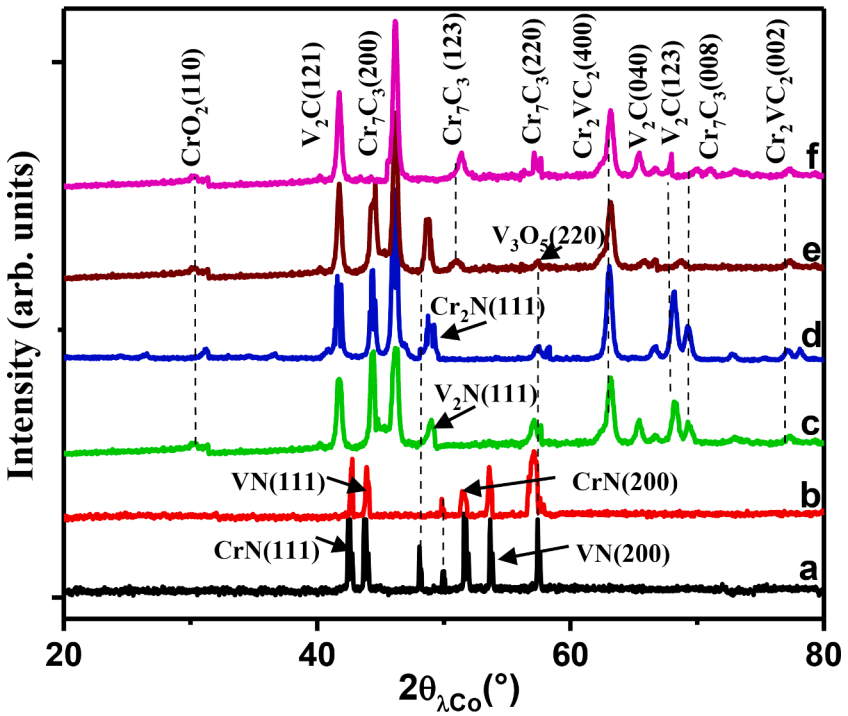

Fig. 2. XRD patterns of Cr-V-C-N coatings deposited under different (N_2 and CH_4) flow rates: a) (20% N_2, 0% CH_4), b) (15% N_2, 5% CH_4), c) (12% N_2, 8% CH_4), d) (10% N_2, 10% CH_4), e) (8% N_2, 12% CH_4), and f) (0 % N_2, 10% CH_4).

possibly related to the decrease in the volume fraction of CrN in the composite coating; as a result of the combination of carbides. Moreover, a slight shift between 531 and 538 cm^{-1} was observed for this band as compared to that obtained from the Cr-V-N coatings (20 % N_2, 0 % CH_4). According to the Raman results, we concluded that the Cr-V-C-N coatings are mainly composed of a mixture of nitride and oxides chromium phasesas reported by Z.B. Qiet al. [3]. The intensity of the VN bands around 445 and 660 cm^{-1} is lower than the CrN bands intensity, suggesting that V atoms occupy vacancies of CrN crystal structure. The vanadium has smaller lattice parameter and lower bands intensity than that of the chromium that facilitates its diffusion into the CrN. A similar result was obtained in our previous study [20].

This behavior can be attributed to the metallic character of the Cr–N bonds. E.C. Romeroet al. [24] have reported a similar behavior in the Cr-Al-N coatings, suggesting that the predominant FCC-CrN structure forms with aluminum inserted through the system Cr-Al-N with the absence of AlN characteristic bands. For the Cr-V-C-N coatings deposited under a mixture of N_2 and CH_4 (except the coating deposited under 15% N_2 + 5%CH_4), the Raman spectra are constituted of two zones with different intensities. The bands in the first zone (200–500 cm^{-1}) are essentially due to the chromium oxides on the coating surface while the bands in the second zone (1000–1500 cm^{-1}) characterize the carbon in different situations. It is clear that the weak peak of CrO_2 is situated at 518 cm^{-1} [24]. The intensity of these peaks increased slightly for the Cr-V-C coating (0% N_2, 10% CH_4) that gives information about the oxidation of the coatings. Also, two carbon peaks were detected: the high peak with sp^2-rich bonded carbon, centered at about 1138 cm^{-1} with a bandwidth of 43 cm^{-1}, as well as a rather broad D peak of sp^3 bonded carbon atoms, centered at about 1343 cm^{-1} with a bandwidth of 60 cm^{-1} [24]. It should be noted that the large of predominant sp^2 and sp^3 bonding peaks means that there are more carbides with high amorphous carbon [25,26]. The broadening of these peaks is due to the high compressive stress generated in the coatings, which is in agreement with C-C bonds detected by Raman analysis in the sputtered Cr-V-C-N [25,27].

3.3. Coating morphology and surface topography

Fig. 4 shows cross section images of Cr-V-C-N coatings deposited on Si (100) wafers under different N_2 and CH_4 flow rates. It has been seen that coatings deposited under (CH_4 + Ar) or (N_2 + Ar) grew quickly and showed higher thickness compared to the Cr-V-C-N coatings deposited under a mixture of (N_2 + CH_4 + Ar). The coatings' thicknesses were between 1230 and 1700 nm (Table 1). The reduction in thickness of coatings deposited under three-gas mixture can be explained by the formation of complex compounds containing C and N atoms on the targets' surfaces where the re-sputtering of these compounds is more difficult than the pure nitride or carbide compounds. A dense and homogenous microstructure was observed for the Cr-V-N coating (Fig. 4 a). Previous studies showed a similar morphology for the Cr-V-N coatings deposited by direct current (DC) unbalanced magnetron sputtering [8].

The Cr-V-C-N coatings presented a dense structure and a good adherence to the substrates. The Cr-V-C coating exhibited a typical columnar microstructure, mostly observed in the magnetron sputtered Me-C coatings [25]. The morphology of Cr-V-C-N coatings does not seem clearly columnar or compacted. In fact, the change in the coating structure is attributed to the high mobility of C through the Cr-V-C-N coatings, which leads to disrupt the columnar grain growth during deposition procedure and hence control the grain size. In our previous study, we observed a similar morphology for the CrN coatings containing a low amount of carbon [5]. Increasing the CH_4 flow rate between 8 and 12% in the deposition chamber led to increase the non-equiaxed columnar growth with a relative dense structure of Cr-V-C-N coatings (Fig. 4 c-e). The coating grains were gradually refined and formed a nanocomposite microstructure. S. K. Ahn et al. [28] have reported a similar morphology for the reactive sputtered Cr-Al-C-N coatings.

Fig. 5 shows 2D AFM images of the Cr-V-C-N coatings. A total area of 3 × 3 μm^2 was scanned to determine the grain size and the surface roughness of the coatings. These results are presented in Table 1. The surface topography of all coatings presented peaks and valleys in nanometric scale and the Rp-V values are in the 15.5–90.6 nm range.

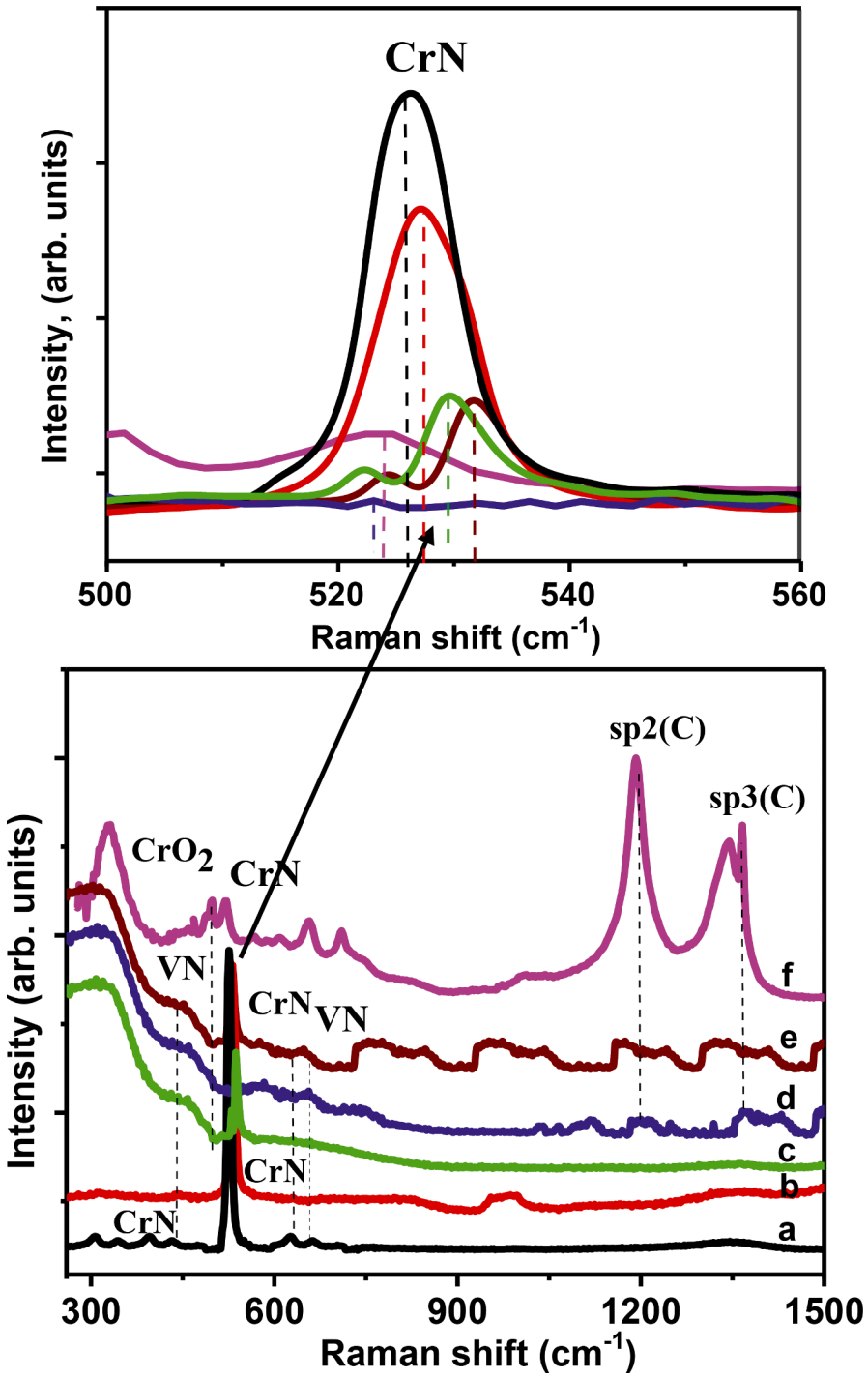

Fig. 3. Raman spectra of Cr-V-C-N coatings deposited under different (N_2 and CH_4) flow rates: a) (20% N_2, 0% CH_4), b) (15% N_2, 5% CH_4), c) (12% N_2, 8% CH_4), d) (10% N_2, 10% CH_4), e) (8% N_2, 12% CH_4), and f) (0% N_2, 10% CH_4).

The Cr-V-N coating was dense and its grains were in facet shape with a crystallite size of about 193 nm presenting a roughness of 21.3 nm (Fig. 5 a). This type of the Cr-V-N topography was previously reported [21, 29]. It has been shown that both roughness and crystallite size of the Cr-V-N coating were lower than these of Cr-V-C coating (42 nm and 245 nm, respectively). Knowing that the enthalpies of formation of CrN, VN and Cr_7C_3 phases are 117.50, 217.15 and 225.60 kJ/mol, respectively, so the formation of the Cr-V-N coating is suggested to require less energy than that of the Cr-V-C coating [8, 30].

From Fig. 5, we can see that the Cr-V-C-N coating surfaces show different topographies as compared to these of Cr-V-N and Cr-V-C coatings. The Cr-V-C-N coating deposited under a gas mixture fewer than 5% CH_4 and 15% N_2 presented a dense and uniform structure with more faceted and elongated grains compared to the Cr-V-N coatings. We notice its low surface roughness (18 nm) and small crystallite size (142 nm) (Table 1, Fig. 5 b). Increasing the CH_4 flow rate up to 12% led to obtain refined coatings with crystallite size reduced from 142 to 46 nm. The low surface roughness (11.1 nm) can be explained by the carbon precipitation into the coatings and the formation of carbides (Fig. 5 d). These results are consistent with the previous studies reported by E. Contreras et al. [8] and S.K. Ahn et al. [28].

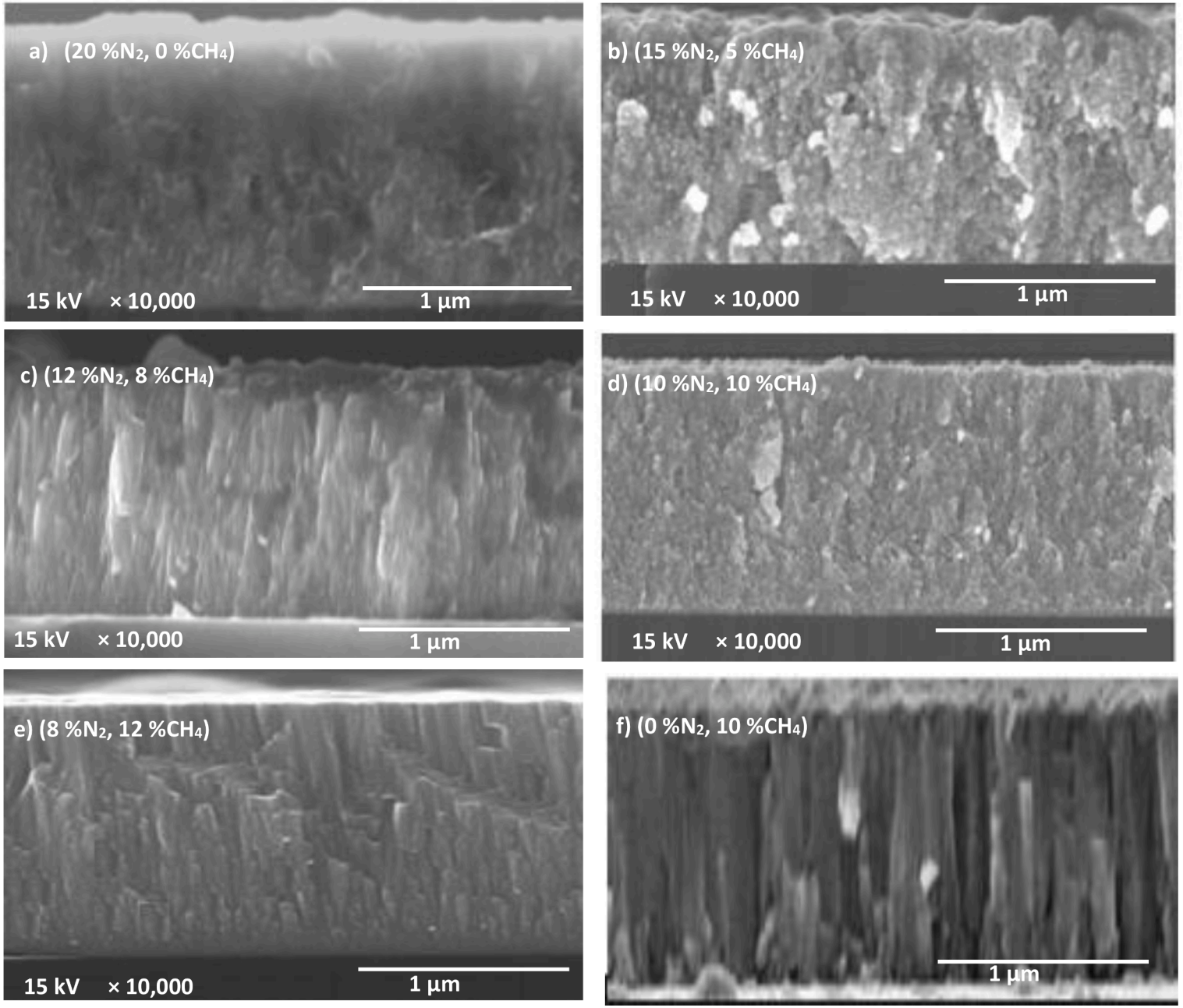

Fig. 4. SEM cross-section images of Cr-V-C-N coatings deposited under different (N_2 and CH_4) flow rates.

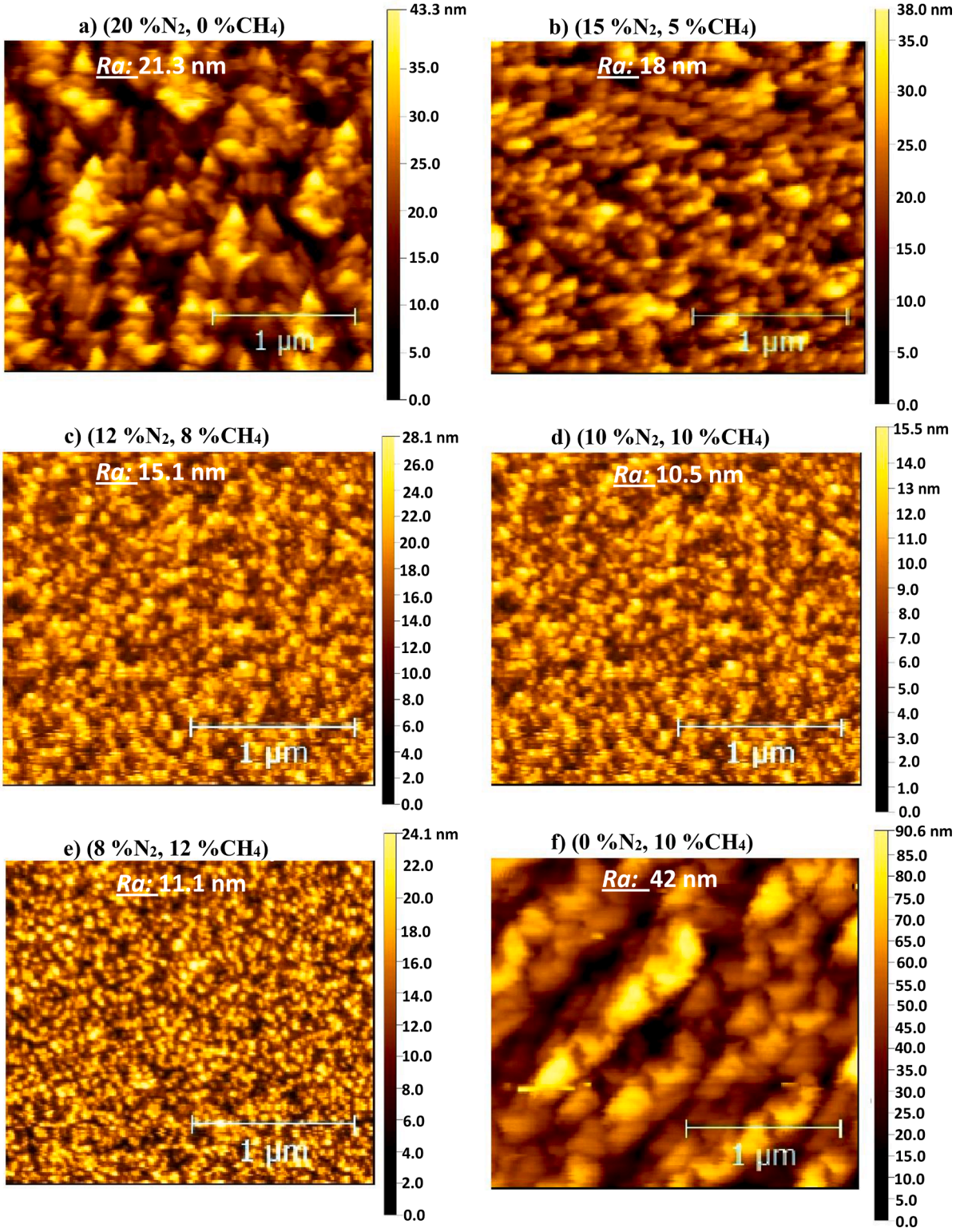

Fig. 5. 2D AFM images of the Cr-V-C-N coatings deposited under different (N_2 and CH_4) flow rates.

3.4. Hardness and Young's modulus

Load–displacement curves and hardness-penetration depth curves of the Cr-V–C–N coatings are shown in Fig. 6. Maximum penetration depth has been limited to a 10% of the coating thickness (namely 80–140 nm) in order to avoid any influence of the substrate [5]. We can clearly notice that the load–unload curves of the Cr-V-N and Cr-V-C coatings are larger than the other curves of Cr-V-C-N coatings. The hardness decreased with increasing the penetration depth down to about 5–8 GPa corresponding to the XC100 steel substrate hardness (Fig. 6 b) [21]. The tendency of the Cr-V-N curves was opposite to the others, which is probably due to the dense structure and nitride-rich regions localized by the indenter. The Cr-V-C-N coating deposited under 10% N_2 and 10% CH_4 flow rate had the maximum hardness value of 28.3 (± 0.6) GPa. It remained constant

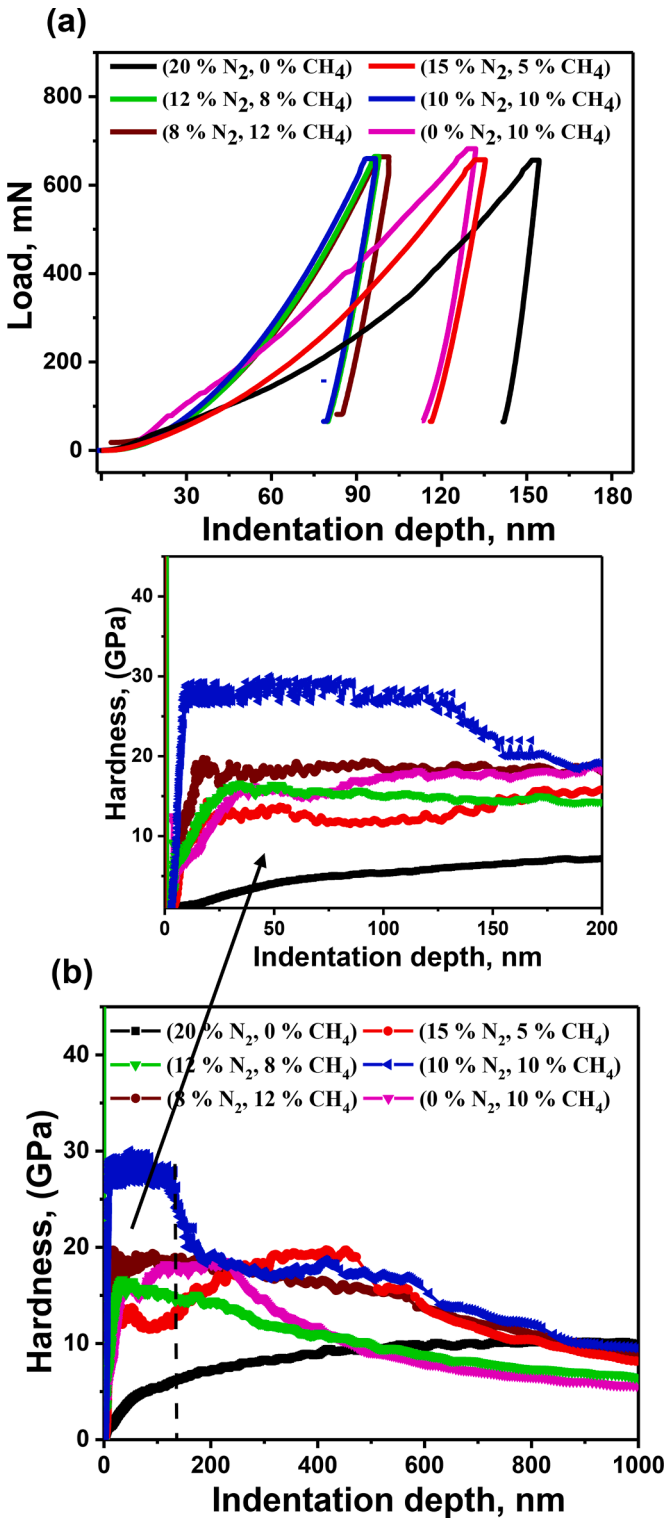

Fig. 6. (a) Nanoindentation load–displacement curves and (b) hardness as a function of the indentation depth for the Cr-V-C-N coatings deposited under different (N_2 and CH_4) flow rates.

for a short distance of 140 nm and then brutally decreased probably because of cracks formed during test [31].

The dependence of coating hardness and Young's modulus on the carbon content is shown in Fig. 7 a. The Cr-V-N coating presented the lowest hardness and Young's modulus: $H = 8.53$ (± 0.4) GPa and $E =$ 134 (±4) GPa. This can be explained by its growth morphology with under-dense regions, large grain size, high surface roughness and low residual stress (-0.4 GPa) [21]. As carbon content in the Cr-V-C-N coatings increased, the coating hardness increased and reached a maximum value of 28.3 (± 0.6) GPa for the coating containing 28 at.% of carbon deposited under 10 % of N_2 and 10 % of CH_4. The hardening of coatings can be explained by the Hall-Petch relation derived from the crystal size refinement. This was simultaneously performed by the co-deposition of carbides phases [28] and the CrN lattice distortion noticed by the shift of peaks, which improves the coating resistance to plastic deformation (solid solution hardening) [13]. However, the measured hardness of 28.3 (± 0.6) GPa is lower than the value given in a previous work reported by S.Y. Heo et al. [16]. The difference between the two hardness values can be explained by the low compressive internal stress in grown coatings [32].

From the point of view of chemical bonding energies, Cr and V elements exist in the Cr-V-C-N as (Cr-N, V-N) nitrides and (Cr-C, V-C, Cr-V-C) carbides, which possibly explain the variation of their hardness. In terms of the crystals' nature of (Cr-N, V-N) nitrides and (Cr-C, V-C, Cr-V-C) carbides, all bonds have covalent characters, and the individual chemical bonding energies of Cr-N, V-N, Cr-C and V-C bonds are (377 ± 18), (448.6 ± 5.8), (277 ± 24) and (373 ± 13) kJ mol^{-1}, respectively [33]. Consequently, the carbides are easier to be formed than the nitrides. Meanwhile, the hardness of Cr_7C_3 and VC phases is higher than that of CrN and VN phases [5,13]. Thus, the presenceof strong carbon bonds like: V–C, Cr-C, sp^2(C) and sp^3(C) can form microcrystals and clusters in the coating. These hard phases can provide a dispersion strengthening function in the coating, which was confirmed by Raman analysis [5,34]. This result indicates that the C-C binding is strongly formed in the Cr-V-C-N coatings after the incorporation of carbon atoms and confirms the coexistence of nitride and carbide phases as shown with XRD analysis. However, further increasing of CH_4 flow rate from 10 to 12% led to an abrupt decrease in the coating hardness to a low value of 20.1 (± 0.4) GPa. This sudden drop in the coating hardness was probably because of the high carbon content (32 at.%). In this case, the higher inter-diffusion of C became more important than that of N. Therefore, the grain boundaries in coatings and dislocations were possibly decreased leading to reduce the hardness. This phenomenon can also be observed from the reduction of the CrN peak intensities in the XRD and Raman analysis (Figs. 2 and 3). The hardness and Young's modulus of Cr-V-C coatings were $H = 18$ (±0.4) GPa and $E = 212$ (± 6) GPa. We notice that the measured hardness is lower than that value obtained by A. Günen et al. (21–25 GPa) [22]. This is due to the Cr_7C_3 and VC phases (C/(Cr+V) = 0.58) and the formation of chromium oxide (7.2% of O) affecting the mechanical properties [21]. From Table 1, we can see that the oxygen content in different coatings is in the 4.4-7.2 at. % range. In our previous studies [20,21], we deposited VN and Cr-V-N films with similar oxygen contents. Moreover, the presence of oxygen in the Cr-V-C-N films induces more local lattice strain, which inhibits the dislocations movement and consequently enhances the strength and hardness of the films [35].

Thus, the hardness of the Cr-V-C-N coating was higher than that of the Cr-V-N coating due to the formation of hard chromium and vanadium carbides. From Fig. 6, we can notice that increasing the C content in coatings from 12.4 to 28 at.% led to increase the coating elasticity modulus from 134 (± 4) to 267(± 6) GPa. Increasing the C content up to 34 at.% led to decrease the Young's modulus to 226 (± 6) GPa.

The hardness/elastic modulus (H^3/E^2) and (H/E) ratios are important parameters which correspond to the durability and the elastic strain to failure, which provide close correlation with wear resistance [22]. These ratios are shown in Fig. 7b. It is clear that the ratios were higher for the most carbon-rich coatings compared to the most nitrogen-rich coatings. Thus, the higher value of H/E and H^3/E^2 indicates the strong coating resistance to plastic deformation. As seen from Fig. 7 b, the Cr-V-C-N coating deposited under 10 % N_2 and 10 % CH_4 shows the highest values: $H/E = 0.0011$ and $H^3/E^2 = 0.1014$ GPa. These results indicate that the Cr-V-C-N coating deposited under 10% N_2 and 10% CH_4 flow rates presents an enhanced toughness with a great potential for

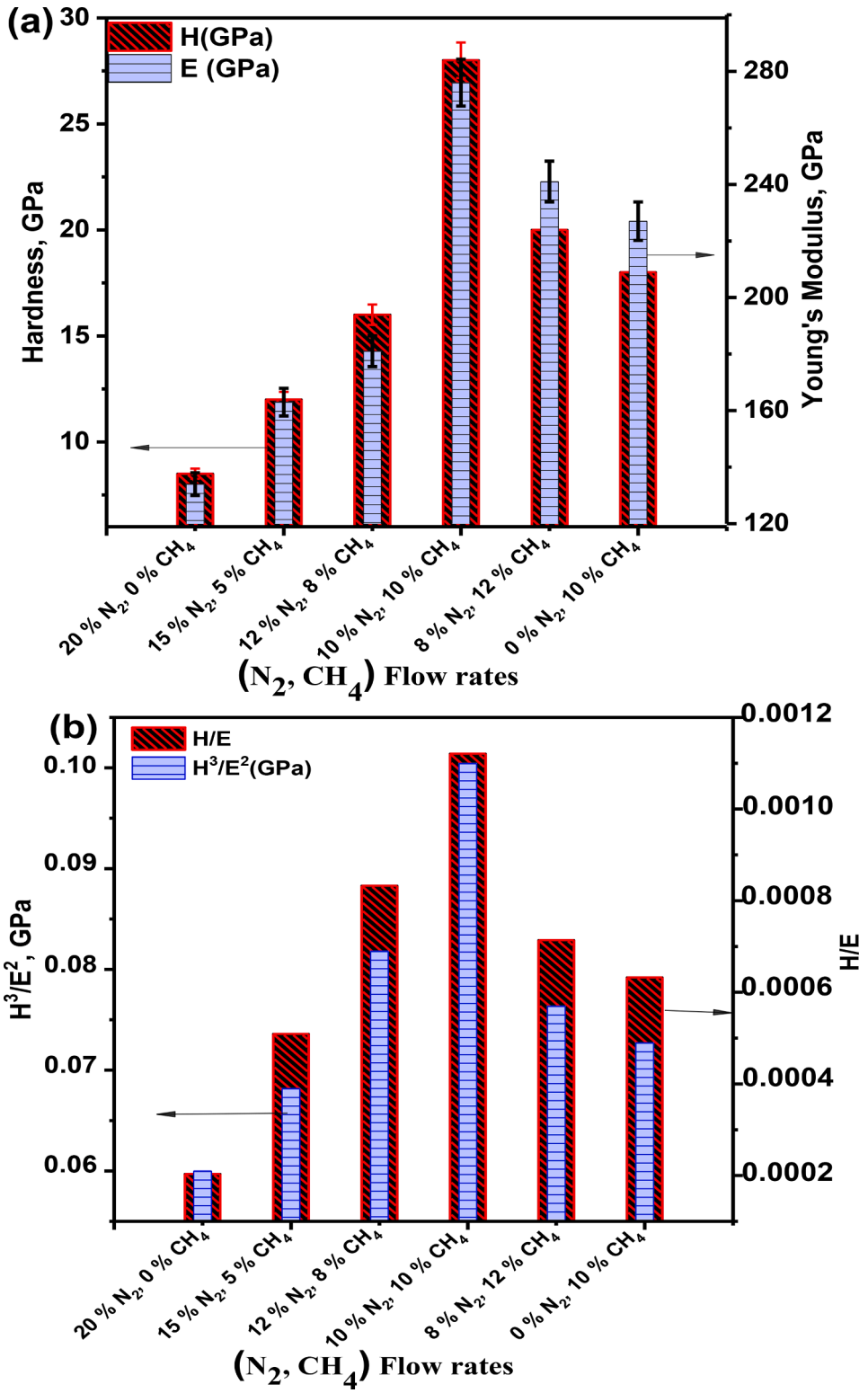

Fig. 7. Mechanical properties of Cr–V–C–N coatings deposited under different (N_2 and CH_4) flow rates: (a) Hardness and Young's modulus, and (b) H/E and H^3/E^2 curves.

the industrial applications [36].

3.5. Tribological properties

3.5.1. Friction coefficient

Fig. 8 shows the evolution of friction coefficients of the Cr-V-C-N coatings deposited under different N_2 and CH_4 flow rates. These curves were recorded during the sliding wear tests using a tribometer in a ball-on-disc configuration. The friction coefficient curves showed two distinct stages. In the first stage (zone I), these curves started at relatively high and instable values at the first contact. This stage can be attributed to the running-in period associated with the contact between the ball and the coating, where the formation of wear debris occurs by the cracking on both counterparts. This stage had a short distance of

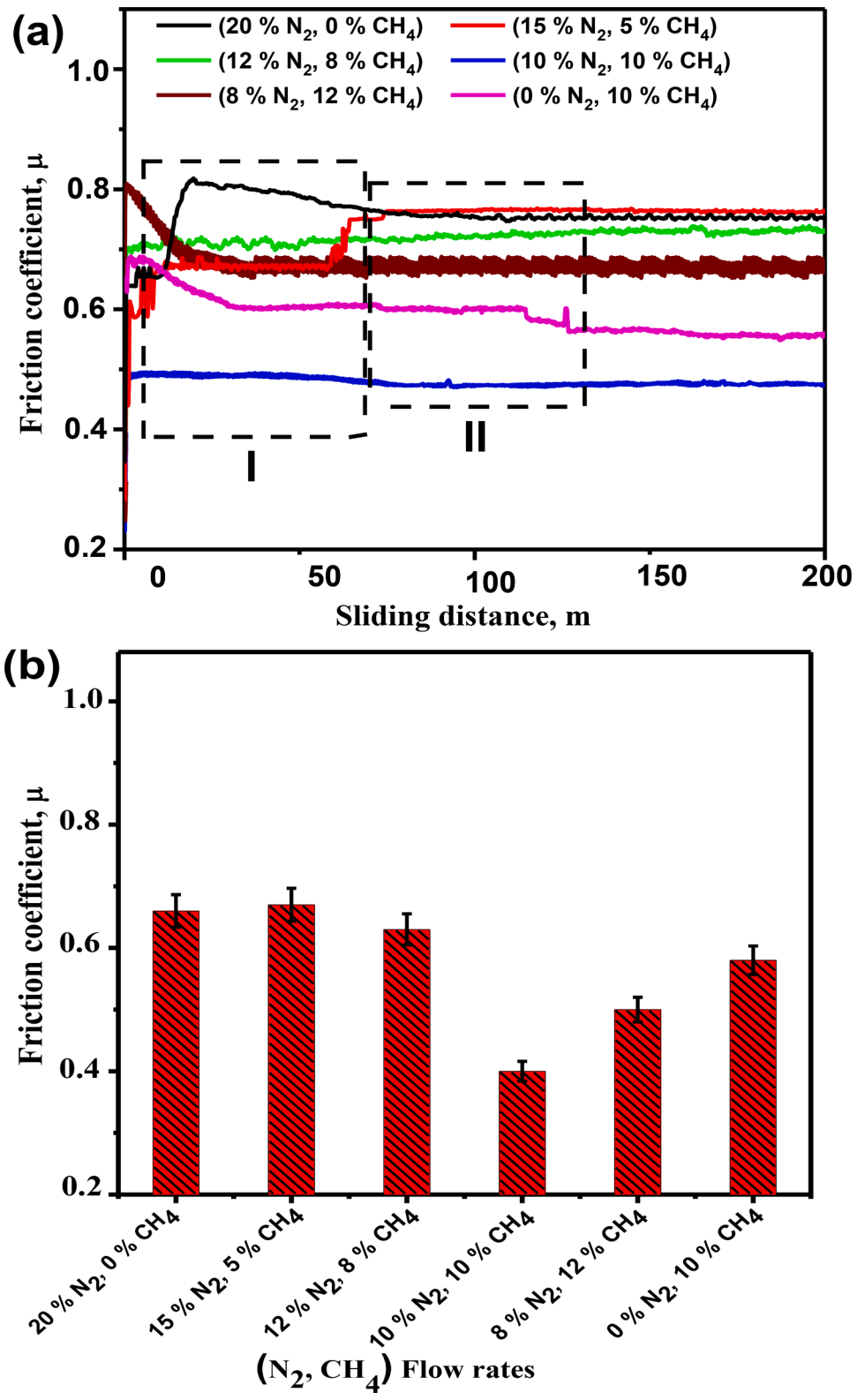

Fig. 8. Friction coefficients of Cr–V–C-N coatings as a function of: a) sliding distance, and b) (N_2 and CH_4) flow rates.

about 60 m then, the friction coefficients decreased to stable values. This is the second stage (zone II) defined as the steady-state friction period beginning after 60 m of sliding distance. The average values of the friction coefficients of coatings were taken from this second stage presenting quasi-constant values. In fact, at the beginning of the test, it is evident that contact surface between the ball and coating presenting high roughness led to the first instable regime (zone I) [37]. The both nitride phases (CrN and VN) of the Cr-V-N coating, with (111) preferred grain plane and the important atomic density caused its low friction coefficient [5]. Cr-V-N coating exhibited a low abrasive resistance with a high friction coefficient of 0.63 (± 0.01) in comparison with that reported in a previous study [22]. This is due to its low hardness and high

surface roughness (Figs. 5 and 7). This relationship was also confirmed in our previous study performed on titanium nitride [38].

Friction and wear properties of Cr-V-C-N coatings were found strongly dependent on the microstructure and the chemical composition. Therefore, the coatings grown at low CH_4 to N_2 ratios showed low hardness values and exhibited a high friction coefficient (0.58–0.60). The increase of carbon content from 12.5 to 28 at.%, corresponding to the increase of CH_4 flow rate from 5 to 10%, led to decrease the coating friction coefficient to its lowest value of 0.47 (± 0.01) (Fig. 8). This low-friction was explained by previous studies where the dense structure and the formation of vanadium compounds play a lubricant role between the two counterparts [34]. On the other hand, the strong dependence of friction and wear resistance on the carbon content can be explained by the incorporation of amorphous carbon in the coatings [39]. The carbon

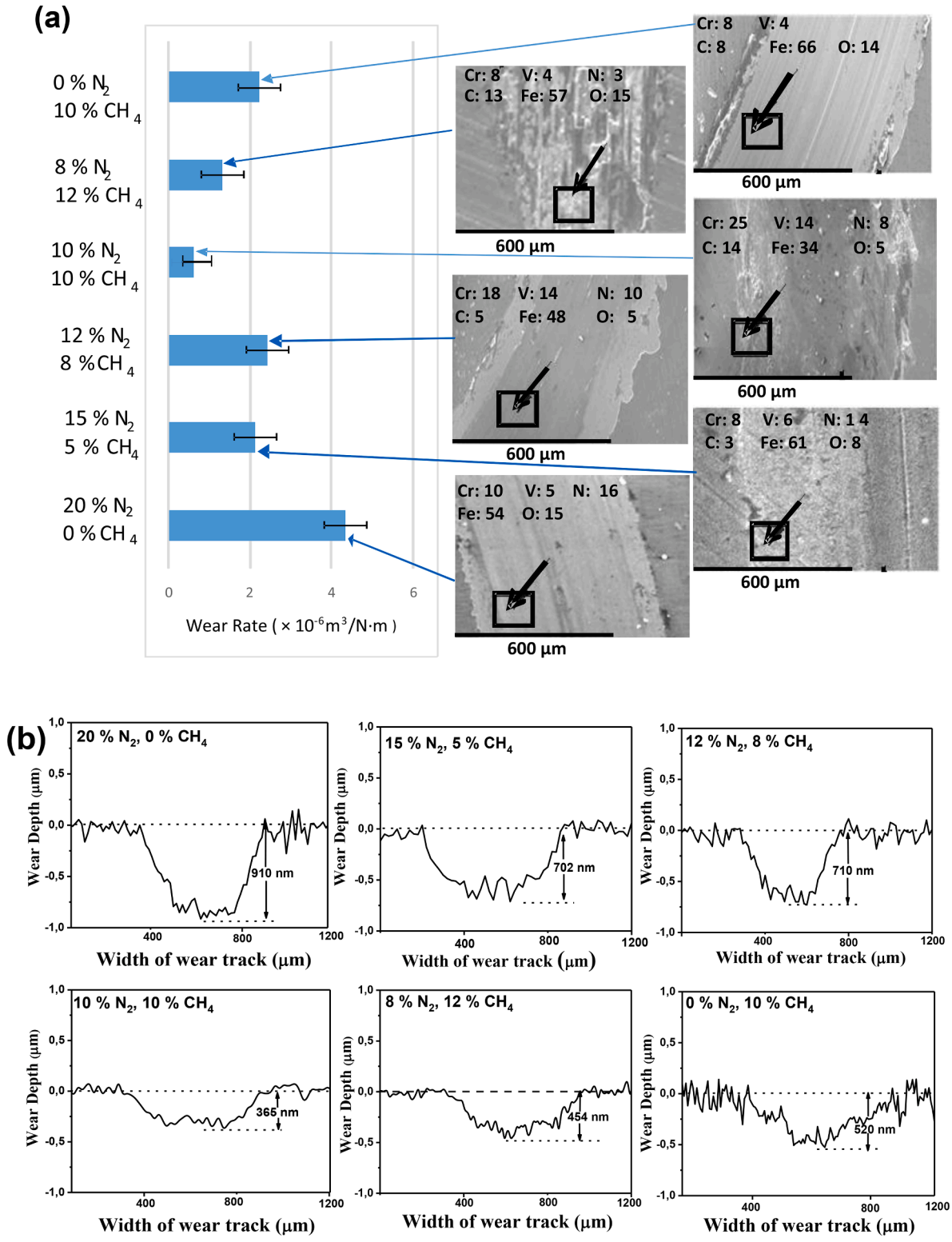

Fig. 9. Evolution of: a) wear rate and b) depth and width of wear tracks of Cr–V–C-N coatings deposited under different (N_2 and CH_4) flow rates.

can make feasible self-adhesion between themselves and the interactions with Cr and V weaken self-adhesion. However, with further increasing of carbon content, the friction coefficient of Cr-V-C-N coatings little increased. It can be seen that the variation of friction coefficient is very similar to the behavior of Cr-Al-C-N coatings deposited by DC unbalanced magnetron sputtering with different carbon contents as reported by E.C. Romero et al. [24].

The Cr-V-C coating had a high friction coefficient of 0.68 because of its carbides phases. The significant difference between the friction coefficients of coatings is related to the variation of coating hardness. The friction coefficient of Cr-V-C coating was lower than that of Cr-V-N coating, which is due to the formation of chromium oxide and lubrication of sp^3 and sp^2 carbon chemical bonding. Meanwhile, the roughness of Cr-V-C coating was higher than that of Cr-V-N coating, which consequently led to enhance the wear resistance of Cr-V-C coating.

3.5.2. *Wear resistance*

Fig. 9 shows the wear rates and the morphologies of wear tracks of the Cr-V-C-N coatings deposited under different N_2 and CH_4 flow rates. The enhancement of the wear resistance of Cr–V–C–N coating was evident with increasing the carbon content in coating. The wear rates of the Cr-V-N and Cr-V-C coatings were 4.33×10^{-6} and $1.64 \times 10^{-6} m^3$/Nm, respectively. With the increase of CH_4 to N_2 ratio, the wear rate of the Cr-V-C-N coating decreased, where the lowest value of $0.67 \times 10^{-6} m^3$/Nm was obtained for the coating containing 28 at.% of carbon (coating deposited under 10% N_2 and 10% CH_4 flow rates) (Fig. 9). The high wear resistance of the Cr–V–C–N coating can be attributed to its dense structure and low surface roughness, which is in agreement with a previous study reported by Y.Mu et al. [34]. The adhesion of coatings to substrates was evaluated by scratch tests (Fig. 9 b). We can see that addition of C through the Cr-V-N coating led to reduce the volume of wear track and adhesion phenomena. These results indicate that doping of Cr-V-N coating with carbon can reduce the interfacial adhesion phenomenon. The high friction coefficient of Cr-V-N coating could be explained by the abrasive effect of coating where a clear delamination and wear debris were observed on the wear tracks with a large track depth of 910 nm and a wide width of 510 nm (Fig. 9). These phenomena showed that wear track zones suffered from plastic deformation with slight abrasive wear before their fatigue fracture.

Increasing the C content in coatings, by increasing the CH_4 flow rate in the deposition chamber, led to decrease the wear track width and thus the friction coefficient. The wear track on the Cr-V-C-N coating containing 28 at.% C (deposited under 10 % N_2 and 10 % CH_4) was smooth and clean with a superficial wear depth of 365 nm and a narrow width of 490. Both the inside and the edge of the wear track were smooth without adhesive failure of the coating. Caicedo et al. investigated the oxidation and the lubrication role of sp^2 carbon bond in the V–C–N coatings [37]. W.Y. Ho et al. found that the improvement of wear resistance of Ti-V-C-N was strongly correlated with the dense structure and chemical composition (high C percentage) [17]. In our case, the excellent wear resistance of the Cr-V-C-N coatings was attributed to the dense structure, high hardness (28.3 ± 0.6 GPa) and fracture toughness (high H/E and H^3/E^2 ratios) as discussed before. This result is similar to that reported by W.Y. Ho et al. [17]. For the Cr-V-C coating, we can see that this coating exhibited a wider wear track with a deep depth of 520 nm (Fig. 9). The inside of the wear track was rough presenting cracks parallel to the sliding direction. In addition, certain adhesive failure can also be observed along the side of the wear track. These observations confirm that the Cr-V-C coating exhibited lower wear resistance as compared to the Cr–V–C–N coatings.

4. Conclusion

In this study, Cr-V-N, Cr-V-C and Cr-V-C-N coatings were deposited by using a radio frequency magnetron sputtering technique with Cr and V targets and reactive N_2 and CH_4 gases. The beneficial effects of carbon addition to Cr-V-N coatings were investigated and can be summarized as follows:

The presence of carbon led to change the chemical composition, microstructural phases, mechanical and tribological properties of the Cr-V-N coatings. Coatings with lower C content presented (CrN and VN) cubic and (Cr_2N and V_2N) hexagonal nitride phases. Increasing the C content in the Cr-V-N coatings led to significantly reduce the nitrides and promote the formation of Cr_7C_3, VC and $CrVC_2$ carbide phases.

Cr-V-C-N coatings containing at least 28 at.% of C revealed the presence of carbide, nitride and carbonitride phases, which resulted in an enhancement in their mechanical properties compared to the Cr-V-N and Cr-V-C coatings.

The $Cr_{0.22}V_{0.21}C_{0.28}N_{0.24}$ coating, deposited under 10% of N_2 and 10% of CH_4 flow rates, was identified as the best alloy presenting the highest hardness of 28.3 GPa, the lowest friction coefficient and wear rate of 0.47 and 7×10^{-7} mm^3/N m, respectively. This coating had sp^3 and sp^2 carbon bonds, which are known for their self-lubricating effect and are responsible for the improvement of coating wear resistance.

5. Credit author statement

Linda Aissani: Conceptualization, Methodology, Writing original.
Akram Alhussein: Conceptualization, Writing review, Validation.
Ahlam BELGROUNE: Methodology, Formal analysis.
Corinne Nouveau: Resources, Writing review, Validation.
Elia Zgheib: Methodology, Software.
Regis Barille: Investigation, Resources.
Alex Montagne: Investigation, Resources.

Declaration of Competing Interest

None.

References

[1] Q. Yuexiu, S. Zhang, B. Li, Y. Wang, J.-W. Lee, F. Li, D. Zhao, Improvement of tribological performance of CrN coating via multilayering with VN, Surf. Coat. Technol. 231 (2013) 126–130.
[2] P.H. Mayrhofer, F. Rovere, M. Moser, C. Strondl, R. Tietema, Thermally induced transitions of CrN thin films, Scr. Mater. 57 (2007) 249–252.
[3] Z.B. Qi, B. Liu, Z.T. Wu, F.P. Zhu, Z.C. Wang, C.H. Wu, A comparative study of the oxidation behavior of Cr_2N and CrN coatings, Thin Solid Films 544 (2013) 515–520.
[4] C. Sabitzer, J. Paulitsch, S. Kolozsvári, R. Rachbauer, P.H. Mayrhofer, Influence of bias potential and layer arrangement on structure and mechanical properties of arc evaporated Al -Cr-N coatings, Vacuum 106 (2014) 49–52.
[5] L. Aissani, M. Fellah, L. Radjehi, C. Nouveau, A. Montagne, A. Alhussein, Effect of annealing treatment on the microstructure, mechanical and tribological properties of chromium carbonitride coatings, Surf. Coat. Technol. 359 (2019) 403–413.
[6] Y.S. Yang, T.P. Cho, H.W. Ye, The effect of deposition parameters on the mechanical properties of Cr–C–Ncoatings, Surf. Coat. Technol. 259 (B) (2014) 141–145.
[7] C.Y. Tong, J.W. Lee, C.C. Kuo, S.H. Huang, Y.C. Chan, H.W. Chen, J.G. Duh, Effects of carbon content on the microstructure and mechanical property of cathodic arc evaporation deposited CrCN thin films, Surf. Coat. Technol. 231 (2013) 482–486.
[8] E. Contreras, Y. Galindez, M.A. Rodas, G. Bejarano, M.A. Gómez, CrVN/TiN nanoscale multilayer coatings deposited by DC unbalanced magnetron sputtering, Surf. Coat. Technol. 332 (2017) 214–222.
[9] J.C. Caicedo, C. Amaya, L. Yate, W. Aperador, G. Zambrano, M.E. Gomez, J. A. Rivera, J.M. Saldan, P. Prieto, Effect of applied bias voltage on corrosion-resistance for $TiC_{1-x}N_x$ and $Ti_{1-x}Nb_xC_{1-y}N_y$ coatings, Appl. Surface Sci. 256 (2010) 2876–2883.
[10] T. Polcar, L. Cvrcek, P. Siroky, R. Novak, Tribological characteristics of CrCN coatings at elevated temperature,, Vacuum 80 (2005) 113–116.
[11] H. Ju, J. Xu, Influence of vanadium incorporation on the microstructure, mechanical and tribological properties of Nb-V-Si-N films deposited by reactive magnetron sputtering, Mater. Charact. 107 (2015) 411–418.
[12] F. Fernandes, A. Loureiro, T. Polcar, A. Cavaleiro, The effect of increasing V content on the structure, mechanical properties and oxidation resistance of Ti-Si-V-N films deposited by DC reactive magnetron sputtering, Appl. Surf. Sci. 289 (2014) 114–123.
[13] L. Aissani, A. Alhussein, C. Nouveau, L. Radjehi, I. Lakdhar, E. Zgheib, Evolution of microstructure, mechanical and tribological properties of vanadium carbonitride coatings sputtered at different nitrogen partial pressures, Surf. Coat. Technol. 374 (2019) 531–540.

[14] S. He, L. Yu, H. Ju, Y. Geng, I. Asempah, J. Xu, Influence of V content on properties of Ti–W–V–N films, Surf. Eng. 35 (1) (2018) 1–8.
[15] K.W. Wang, T.N. Lin, D.Y. Wang, Tribological property enhancement of CrN films by metal vapor vacuum arc implantation of vanadium and carbon ions, Thin Solid Films 516 (6) (2008) 1012–1019.
[16] S.Y. Heo, J.H. Shin, D.I. Kim, J.Y. Oh, S.H. Zhang, K.H. Kim, Microstructure and mechanical properties of Cr–V–C–N films, Surf. Eng. 31 (7) (2014) 513–518.
[17] W.Y. Ho, M.D. Chen, C.L. Lin, W.Y. Ho, Characteristics of TiVN and TiVCN coatings by cathodic arc deposition,, in: 6th International Conference on Mechatronics, Materials, Biotechnology and Environment, 2016, pp. 597–601 (ICMMBE).
[18] L.R. Constantin, A.C. Parau, M. Balaceanu, M. Dinu, A. Vladescu, Corrosion and tribological behaviour in a 3.5% NaCl solution of vacuum arc deposited Zr-C-N and Zr–Cr–Si–C–N coatings, J. Eng. Tribol. (2018) 1–12.
[19] D. Nath, F. Singh, R. Das, X-ray diffraction analysis by Williamson-Hall, Halder-Wagner and size-strain plot methods of CdSe nanoparticles- a comparative study, Mater. Chem. Phys. 239 (2020), 122021.
[20] L. Aissani, A. Alhussein, C. Nouveau, L. Ghelani, M. Zaabat, Influence of film thickness and Ar-N_2 plasma gas on the structure and performance of sputtered vanadium nitride coatings, Surf. Coat. Technol. 378 (2019), 124948.
[21] L. Aissani, C. Nouveau, M.J. Walock, H. Djebaili, A. Djelloul, Influence of vanadium on structure, mechanical and tribological properties of CrN coatings, Surf. Eng. 31 (10) (2015) 779–788.
[22] A. Günen, B. Kurt, P. Milner, M.S. Gök, Properties and tribological performance of ceramic-base chromium and vanadium carbide composite coatings, Int. J. Refractory Metals Hard Mater. 81 (2019) 333–344.
[23] B. Kaplan, A. Blomqvist, C. Arhammar, M. Selleby, S. Norgren, Structural determination of $(Cr,Co)_7C_3$,, in: 18th Plansee Semin. Reutte, Austria, 2013, pp. 1–12.
[24] E.C. Romero, M.G. Botero, W. Tillmann, F.B. Osorio, G.B. Gaitán, Influence of carbon content on the microstructure, mechanical and tribological properties of CrAlCN coatings deposited by DC unbalanced magnetron sputtering, Bull. Mater. Sci. 41 (97) (2018) 2–10.
[25] K. Nygren, M. Samuelsson, A. Flink, H. Ljungcrantz, A.K. Rudolphi, U. Jansson, Growth and characterization of chromium carbide films deposited by high rate reactive magnetron sputtering for electrical contact applications, Surf. Coat. Technol. 260 (2014) 326–334.
[26] G. Gassner, P.H. Mayrhofer, E. Hegedus, L. Tóth, I. Kovacs, B. Pécz, V. Srot, Ch. Scheu, C. Mitterer, Structure of sputtered nanocomposite CrCx /a-C:H thin films, J. Vac. Sci. Technol. B 24 (4) (2006) 1837–1843.
[27] J. Schwan, S. Ulrich, V. Batori, H. Ehrhardt, Raman spectroscopy on amorphous carbon films, J. Appl. Phys. 80 (1996) 440–445.
[28] S.K. Ahn, S.H. Kwon, K.H. Kim, Effect of carbon on microstructure of $CrAlC_xN_{1-x}$ coatings by hybrid coating system, Trans. Nonferrous Met. Soc. China. 21 (2011) 78–82.
[29] Y.X. Qiu, B. Li, J.W. Lee, D.L. Zhao, Self-lubricating CrVN coating strengthened via multilayering with VN, J. Iron Steel Res. Int. 21 (5) (2014) 545–550.
[30] W.M. Dawson, F.R. Sale, Comparison of the activation energies of the formation of chromium carbide coating on carburized and uncarburized AISI 1020 steel, Metallurgical Transactions A8 (1) (1977) 15–18.
[31] Q. Wang, F. Zhou, J. Yan, Evaluating mechanical properties and crack resistance of CrN, CrTiN, CrAlN and CrTiAlN coatings by nanoindentation and scratch tests, Surf. Coat. Technol. 285 (2016) 203–213.
[32] H. Ichimura, I. Ando, Mechanical properties of arc-evaporated CrN coatings: Part I nanoindentation hardness and elastic modulus, Surf. Coat. Technol. 145 (2001) 88–93.
[33] Y.R. Luo, Comprehensive Handbook of Chemical Bond Energies, CRC Press, Boca Raton, FL, 2007.
[34] Y. Mu, M. Liu, Y. Zhao, Carbon doping to improve the high temperature tribological properties of VN coating, Tribol. Int. 97 (2016) 327–336.
[35] F. Vaz, J. Ferreira, E. Ribeiro, L. Rebouta, S. L-Mendez, J.A. Mendes, E. Alves, Ph. Goudeau, J.P. Rivière, F. Ribeiro, I. Moutinho, K. Pischow, J. de Rijk, Influence of nitrogen content on the structural, mechanical and electrical properties of TiN thin films, Surf. Coat. Technol. 191 (2005) 317–323.
[36] J. Lin, John J. Moore, B. Mishra, M. Pinkas, X. Zhang, W.D. Sproul, CrN/AlN superlattice coatings synthesized by pulsed closed field unbalanced magnetron sputtering with different CrN layer thicknesses, Thin Solid Films 517 (2009) 5798–5804.
[37] J.C. Caicedo, W. Aperador, C. Amaya, Determination of physical characteristic in vanadium carbon nitride coatings on machining tools, Int. J. Adv. Manuf. Technol. 91 (1-4) (2016) 1227–1241.
[38] L. Aissani, A. Alhussein, A. Ayad, C. Nouveau, E. Zgheib, A. Belgroune, M. Zaabat, R. Barille, Relationship between structure, surface topography and tribo-mechanical behavior of Ti-N thin films elaborated at different N_2 flow rates, Thin Solid Films 724 (2021), 138598.
[39] C.A. Charitidis, E.P. Koumoulos, D.A. Dragatogiannis, Nanotribological behavior of carbon based thin films: friction and lubricity mechanisms at the nanoscale, Lubricants 1 (2013) 22–47.